Materials Science-Poland, 37(4), 2019, pp. 547-553
http://www.materialsscience.pwr.wroc.pl/
DOI: 10.2478/msp-2019-0077

sciendo

Synthesis, morphology, electrical conductivity and electrochemical properties of α-Ni(OH)$_2$ and its composites with carbon

O.M. KHEMII, I.M. BUDZULIAK, V.O. KOTSYUBYNSKY*, L.S. YABLON, R.V. ILNYTSKYI, V.M. BOYCHUK, O.V. MORUSHKO, KH.V. BANDURA, M.M. KHEMII

Vasyl Stefanyk Precarpathian National University, 57 Shevchenko St., Ivano-Frankivsk, 76025, Ukraine

A simple and effective hydrothermal synthesis of spherical α-Ni(OH)$_2$ particles and α-Ni(OH)$_2$/carbon composites was proposed. The mechanism of ultrafine α-Ni(OH)$_2$ phase forming and correlations between synthesis conditions, morphology, electrical conductivity were analyzed. It was found that carbon nanoparticles form an electric conductive cover on nickel hydroxide microparticles during synthesis which increases overall electronic conductivity of the composite material. α-Ni(OH)$_2$ and α-Ni(OH)$_2$/C samples were tested as electrodes for hybrid supercapacitors. It was found that carbon coverings stabilize α-Ni(OH)$_2$ phase in the alkaline medium. The comparison of the influence of laser irradiation and ultrasonic treatment on the electrochemical performance of the obtained materials was made.

Keywords: *nickel hydroxide; electrical conductivity; specific capacitance; diffusion of charge carriers.*

1. Introduction

Increasing of specific power and capacitance is of highest priority for the further development of modern electrochemical systems. The main direction is finding advanced materials with an effective combination of physical and chemical properties. The main requirements for high performance electrode material are the following: crystal structure with the presence of guest positions for alkaline ions intercalation, high electrical conductivity, large specific surface area, and required pore size distribution, chemical inertness to electrolytes, low price, and ecological safety. Nanoporous carbon is a typical electrode material for symmetric supercapacitors. Another promising solution is an asymmetric hybrid supercapacitor (HS) that combines a non-Faradaic double-layer capacitive electrode based on activated carbon with a transition metal oxide electrode. Layered transition metal hydroxides and sulfides are the promising electrode materials for HS [1–4]. Among them ultrafine nickel hydroxide is attractive for investigations due to its structural and electronic properties. It is known that Ni(OH)$_2$ (both α- and β-modifications [5]) has hexagonal brucite-type structure with Ni(OH)$_2$ layers arranged along *c* crystallographic axis, where Ni^{2+} ions occupy the octahedral positions. The investigations of synthesis conditions effect on the structural, morphological, electrical and electrochemical properties of ultrafine α-Ni(OH)$_2$ and α-Ni(OH)$_2$/carbon (α-Ni(OH)$_2$/C) are important for obtaining high performance electrode materials.

2. Experimental

The nickel hydroxide was synthesized by a hydrothermal route. Both nickel hexahydrate nitrate (0.626 g) and urea (2.584 g) were dissolved in 100 mL of distilled water and hydrothermally treated in the Teflon-lined stainless steel autoclave for 5 hours at the temperature of 90 °C. The obtained precipitate was washed with distilled water and ethanol till neutral pH was achieved and then dried at the temperature of 60 °C for 12 hours (S0 sample). Hydrothermal synthesis of Ni(OH)$_2$/C composite was carried out under the same conditions with adding of nanoporous carbon

*E-mail: kotsuybynsky@gmail.com

(60 mg) to the reaction medium [6]. Three samples of $Ni(OH)_2$/C composites were obtained. Sample S1 and sample S3 were synthesized using α-$Ni(OH)_2$/C colloidal solution previously ultrasonicated for 120 min and 25 min, respectively. S2 sample was obtained by hydrothermal treatment of α-$Ni(OH)_2$/C after laser irradiation for 3 min. Ultrasonic treatment was performed at a frequency of about 25 kHz. YAG:Nd^{3+} laser (1.06 μm, Q-switching mode) was used for the experiments.

The following chain reactions proceed in the hydrothermal process:

$$CO(NH_2)_2 + H_2O \rightarrow 2NH_3 + CO_2 \quad (1)$$

$$NH_3 + H_2O \leftrightarrow NH^{4+} + OH^- \quad (2)$$

$$CO_2 + H_2O \leftrightarrow 2H^+ + CO_3^{2-} \quad (3)$$

$$CO(NH_2)_2 \rightarrow NCO^- + NH_4^+ \quad (4)$$

$$Ni^{2+} + yNH_3 \cdot H_2O \leftrightarrow [Ni(NH_3)_y]^{2+} + yH_2O \quad (5)$$

$$[Ni(NH_3)_y]^{2+} yOH^- \leftrightarrow [Ni(OH)_y]^{(y-2)^-} + yNH_3 \quad (6)$$

$$[Ni(OH)_y]^{(y-2)^-} \rightarrow Ni(OH)_2 \downarrow + H_2O \quad (7)$$

According to reaction 1 urea thermal decomposition runs at 100 °C, resulting in NH_3 and CO_2 OH^- and CO_3^{2-} ions which are the products of hydrolysis (reaction 2 and reaction 3). NCO^- ions formation is also possible in urea hydrolysis (reaction 4). Ni^{2+} ions absorption on the carbon particles during hydrothermal synthesis of the composite takes place. $[Ni(NH_3)_y]^{2+}$ complex formation is a result of interaction of Ni^{2+} ions and ammonia (reaction 5). The surfaces of carbon particles with absorbed Ni^{2+} ions are heterogeneous centers for $Ni(OH)_2$ particles nucleation and anisotropic growth (reaction 6 and reaction 7).

3. Results

According to XRD data all the synthesized samples form only a hexagonal α-$Ni(OH)_2$ phase (a = 0.308 nm and c = 2.341 nm) that corresponds to JCPDS Card No. 38-0715 [7, 8]. The layered structure of α-$Ni(OH)_2$ contains the stack of positive charged layers of $Ni(OH)_{2-x}$ with anions and water molecules intercalated into the interlayer space [9]. Ni^{2+} ions on the (0 0 1) surface are linked with OH^- and Ni^{2+} ions located on adjacent surfaces and isolated by OH^- layers. There is a weak interaction between the layers and a strong one between the stacks of $Ni(OH)_2$ crystals with layered structure, thus, the energy of the layered (0 0 1) surface is minimal. Surface free energy is minimal when the open facets are built with lower-energy (0 0 1) surfaces for $Ni(OH)_2$. As a result nickel hydroxide growth can be observed mostly along the (0 0 1) surface [10]. These structural peculiarities determine XRD patterns. Intensive diffraction peaks for (0 0 3), (0 0 6) and (0 0 9) planes are observed (Fig. 1). The broadening and asymmetry of the peaks for $2\theta > 30°$ are caused by the local disordering of layers. XRD patterns of all $Ni(OH)_2$/C samples are very similar with the intensity increasing for $2\theta > 20°$ due to the presence of amorphous carbon (Fig. 1).

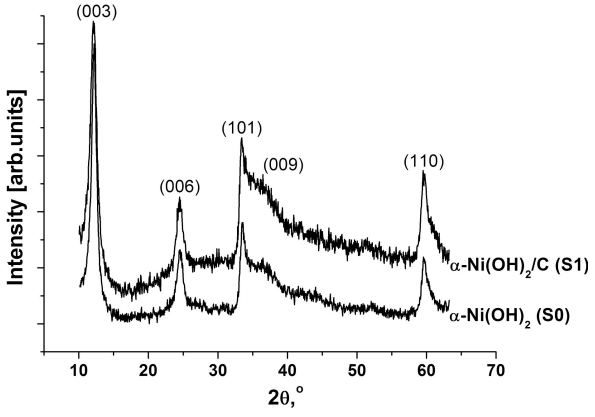

Fig. 1. XRD patterns of α-$Ni(OH)_2$ (S0) and $Ni(OH)_2$/C composite (S1) samples.

The morphology of the synthesized materials was analyzed using scanning electron microscopy (SEM). S0 sample is composed of α-$Ni(OH)_2$ microspheres with an average size of about 4 μm

(Fig. 2a). It was found that the formation of carbon covering $Ni(OH)_2$ particles for all carbon-containing samples does not depend on the synthesis conditions (Fig. 2b). This result is in a good agreement with an assumption about Ni^{2+} ions absorption on the carbon nanoparticles during the hydrothermal treatment.

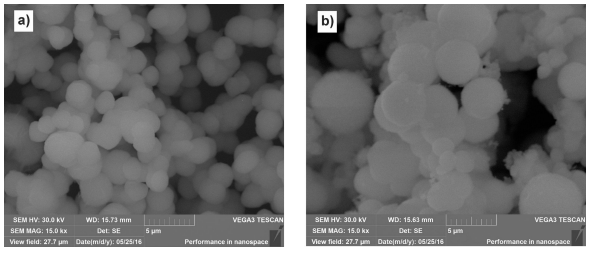

Fig. 2. SEM images of α-$Ni(OH)_2$ (S0) and $Ni(OH)_2$/C composite (S1) samples.

The frequency response of electrical conductivity of the synthesized materials was investigated by electrochemical impedance spectroscopy (EIS). Frequency dependence of electrical conductivity $\sigma_{AC}(\omega)$ of α-$Ni(OH)_2$ can be described [11] as:

$$\sigma_{AC}(\omega) = \sigma_{DC} + \sigma_{pol}(\omega) \tag{8}$$

where $\sigma_{pol}(\omega)$ is a polarization-based component and σ_{DC} is a direct current conductivity. Ionic conductivity of $Ni(OH)_2$ can be described by Nernst-Einstein model with a hopping mechanism of charge transport in the particular dynamic bond percolation (DBP) model [12]. The DBP model assumes that the ions between the nearest adjacent sites are separated by potential barriers. The diffusion coefficient of ions is given by the Einstein-Smoluchowski equation for the random-walk diffusion model with a charge transfer via hopping mechanism [11]. Protons diffusion and dipoles orientation for α-$Ni(OH)_2$ phase are controlled by intercalated water molecules. The model of diffusion-limited ionic conductivity of α-$Ni(OH)_2$ based on protons transition through the intermediary OH^- groups can be proposed. (Fig. 3a).

For β-$Ni(OH)_2$ phase the diffusion of protons and dipole reorientation take place only between the localized proton defects and the protons do not take part in hydrogen bonds formation (Fig. 3b).

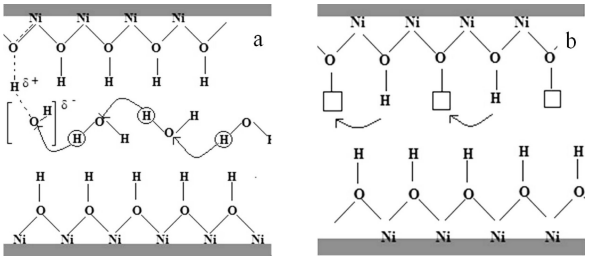

Fig. 3. Schematic representation of proton moving in α-$Ni(OH)_2$ (a); and β-$Ni(OH)_2$ (b) [13].

The experimental frequency dependence of conductivity $\sigma(\omega)$ of α-$Ni(OH)_2$ is typical of disordered semiconductors: slight changes in low-frequency region and exponential growth at the high frequencies (Fig. 4).

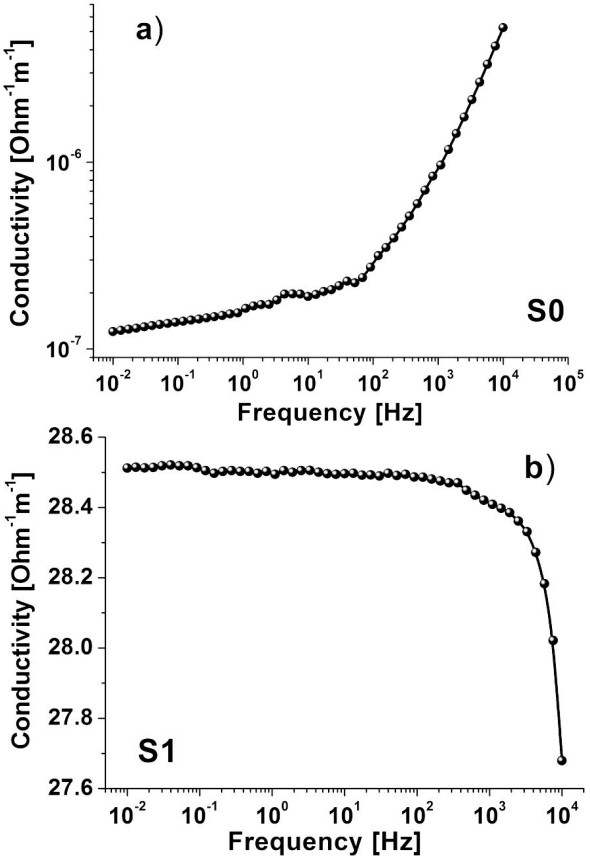

Fig. 4. Frequency dependence of the electrical conductivity of α-$Ni(OH)_2$ (S0) and $Ni(OH)_2$/C (S1) samples.

For low-ordered systems DC and AC components of electrical conductivity follow the same

mechanism. The observed exponential growth of the electrical conductivity is typical of semiconductor materials with percolation mechanism of charge transfer [14]. For interpretation of electrical-relaxation phenomena for DC and AC components of conductivity, Jonscher power law was used:

$$\sigma(\omega) = \sigma_{dc}\left[1 + \left(\frac{\omega}{\omega_h}\right)^s\right] \qquad (9)$$

where ω_h is a hopping frequency of charge carriers and s is the frequency exponent parameter in the range of $0 < s < 1$ (s is a measure of deviation from Debye behavior and of the interionic coupling strength) [15]. This model is used for describing the non-Debye relaxation in solids during generation-recombination processes that involve localized states within the band-gap, phonon-controlled jumps of electrons or ions at non-ordered potential inside the electric field and also spontaneous polarization. The specific electrical conductivity of $Ni(OH)_2$/C composite materials sharply decreases at frequencies higher than 1 kHz (Fig. 4b).

Low-frequency specific conductivity of the composite material is more than 7 orders higher than for pure α-$Ni(OH)_2$ due to electronic conductivity of carbon material. The lack of changes in conductivity in the frequency range of 10^{-2} Hz to 10^3 Hz can be explained by the conductive carbon chains formation between α-$Ni(OH)_2$ particles [16]. The next decrease in specific conductivity of the composite materials is caused by skin-effect or collective perturbations of the charge density in the fine-dispersed conductive systems [17, 18]. At the same time, the porous structure of carbon provides the charge carriers delocalization so the changes in the carbon material microstructure and morphology are controlling its conductivity and electrochemical properties. Electrical conductivity of carbon depends on the number of atoms in sp^2-hybridized state. Thermal processing can be used for electrical conductivity enhancement with simultaneous structure ordering [19].

Cyclic voltammetry (CVA) was used for calculation of specific capacitance of the obtained materials. Approximately 10 mg of each sample was pressed into Ni foam (without using any carbon black additives) for electrochemical investigation in a three-electrode beaker cell with Ag/AgCl (in 3 M KCl) reference electrode, Pt counter electrode and 1 M KOH aqueous electrolyte. Fig. 5 shows CVA curves of $Ni(OH)_2$ and $Ni(OH)_2$/C composite at different stages of cycling at the same scan rates (1 mV/s). The pseudocapacitive properties of all the electrodes have been revealed.

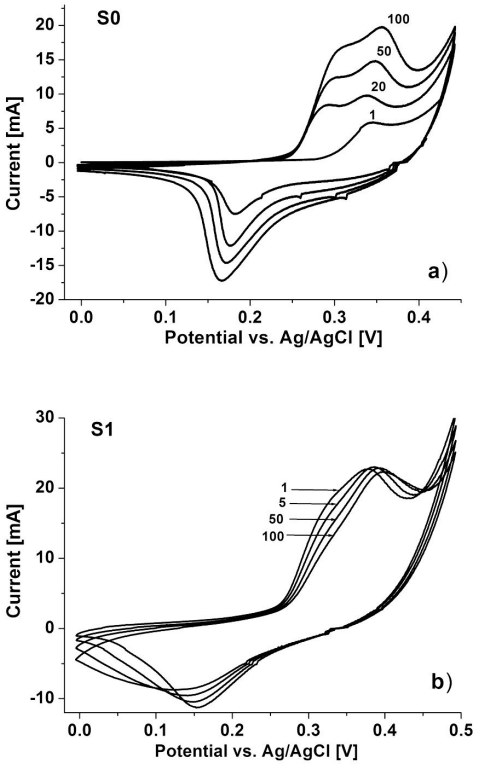

Fig. 5. CVA curves of α-$Ni(OH)_2$ (S0) and α-$Ni(OH)_2$/C composites (S1, S2, S3) at a scan rate of 1 mV/s.

The redox current peaks corresponding to the reversible transition of Ni^{2+} to Ni^{3+} are observed. Two peaks on the CVA anode branches of $Ni(OH)_2$ (sample S0) in the ranges of 0.28 V to 0.31 V and 0.33 V to 0.35 V can be explained by the presence of amorphous β-$Ni(OH)_2$ additives [20]. However, there are no symmetric peaks on the cathode branch, which means that the kinetic properties of Ni^{3+} reduction for both phases are very similar. It was found that anode current peak for S0 sample

shifts to the positive potential. α-Ni(OH)$_2$ phase is thermodynamically unstable, thus, the most possible reason for that is the shift to more stable β-Ni(OH)$_2$ phase. α-Ni(OH)$_2$ phase transformation occurs during two parallel processes: transition to the β-Ni(OH)$_2$ in the concentrated KOH solution and electrochemical redox cycling. α → β phase transfer is accompanied by a loss of water molecules and surface redox reactions defined by protons diffusion. Oxidation of Ni^{2+} to Ni^{3+} is accompanied by the solid-state proton intercalation/deintercalation and the observed anode current growth is a result of protons mobility increasing. Therefore, the conditions of proton diffusion affect the redox reactions during Ni(OH)$_2$ phase transformation. Polarized hydrogen ions move to the Ni(OH)$_2$/electrolyte interface at the anode: $(OH^-)_V \leftrightarrow (OH^-)_S$, where V is the electrolyte volume and S is a surface of the electrode. The next step is hydroxyl ions diffusion from the superficial layers of Ni(OH)$_2$ particles to the bulk: $(OH^-)_S \leftrightarrow (OH^-)_B$. Protons formed in the oxidation processes move into Ni(OH)$_2$ structure and interact with OH^- groups forming water molecules: $(H^+)_B \rightarrow (H^+)_n$ and $(H^+)_n + (OH)^-_n \rightarrow (H_2O)_n$. Neutral area expands to Ni(OH)$_2$/electrolyte interface. This effect explains the presence of internal water concentration gradient [21].

The shift of anode peaks to more positive potential for α-Ni(OH)$_2$/C composite (S1 sample) is observed. There is no splitting of peaks in this case so α-Ni(OH)$_2$ phase remains stable in the redox process in the presence of carbon component.

Fig. 6 shows the CVA curves for all the synthesized samples in the same electrolyte at different scan rates. All the curves include a pair of redox peaks indicating that the capacitance characteristics are caused by Faradaic reactions. The anodic and the cathodic peak currents increase with the scan rate increasing.

For reversible semi-infinite diffusion-controlled processes, the peak current values are linearly dependent on the square root of potential scan rate, when for the adsorption processes the peak current values are directly proportional to the potential scan rate [22].

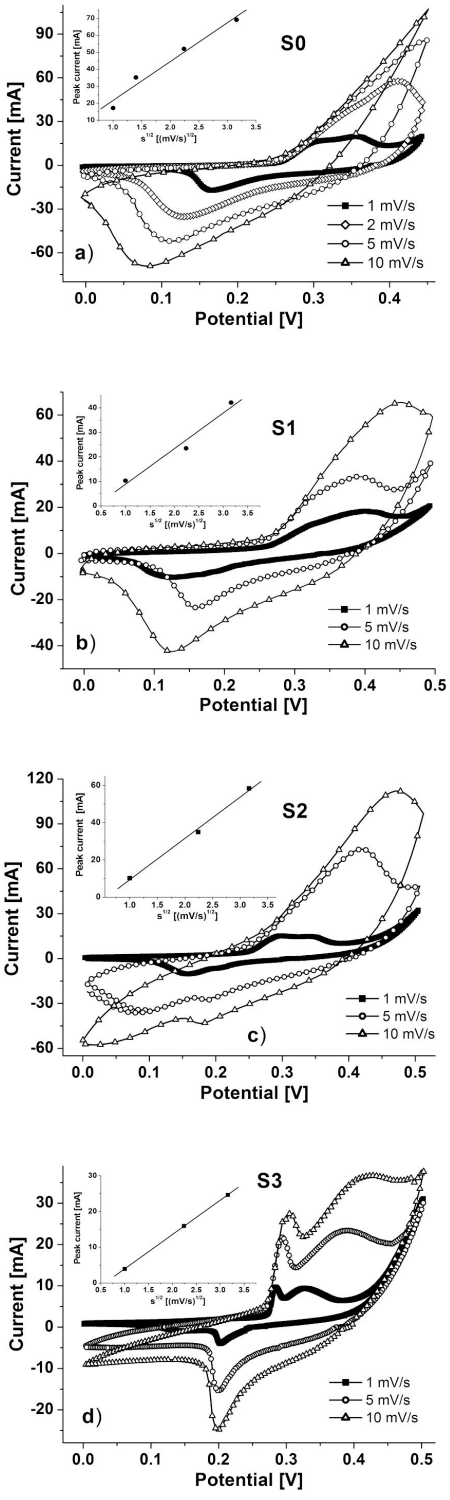

Fig. 6. CVA curves of α-Ni(OH)$_2$ (a); and α-Ni(OH)$_2$/C (b), (c) and (d) (plots of peak current changes with square root of scan rates are in the insets).

The linear dependence between the peak current and $s^{0.5}$ was found for all the materials confirming that the oxidation of nickel hydroxide is diffusion limited for all the cases. According to Randles-Shevchik equation, angular coefficient k of $i_n(s^{1/2})$ linear dependencies are proportional to proton diffusion coefficient. It was found that this parameter is equal 22.88 A·s/V^{-1} for α-Ni(OH)$_2$ and 14.54 A·s/V^{-1}, 22.21 A·s/V^{-1} and 9.6 A·s/V^{-1} for S1, S2 and S3 α-Ni(OH)$_2$/C samples, respectively. The diffusion coefficient is the highest for S0 (α-Ni(OH)$_2$) and for S2 sample (α-Ni(OH)$_2$/C composite after laser treatment) and the lowest for the S3 sample (α-Ni(OH)$_2$/C composite after ultrasound-processing). CVA curves for S2 and S3 samples have an additional peak on the anode branches so both α- and β-phases of Ni(OH)$_2$ are present. It can be assumed that the changes in carbon nanoparticles size due to ultrasonic treatment are insufficient for its penetration into Ni(OH)$_2$ interlayer space. The calculated average specific capacitance is the highest for Ni(OH)$_2$/C composite (S1 sample): about 310 F/g (Fig. 7). The lowest specific capacitance that corresponds to the lowest value of diffusion coefficient, was obtained for α-Ni(OH)$_2$/C after long ultrasound-processing.

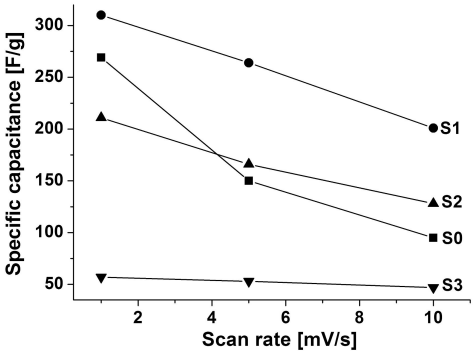

Fig. 7. Dependence of specific capacitance on scan rate for the synthesized materials

EIS was used for α-Ni(OH)$_2$ and α-Ni(OH)$_2$/C composite electrodes investigation. The Nyquist plots showed semicircles in high frequency area and a close to linear behavior in low frequency range which corresponds to Warburg impedance of diffusion-controlled charge transfer (Fig. 8). The characteristics of the electrochemical system can be represented by the electrical equivalent circuit (Fig. 8, inset). It is known that an increase in semicircle diameter is caused by an increase in the charge-transfer resistance and the higher slope is a result of lower diffusion rate. The slope at low frequencies is interpreted as an empirical parameter related to the diffusion resistance where the greater inclination means the lower diffusion mobility [23].

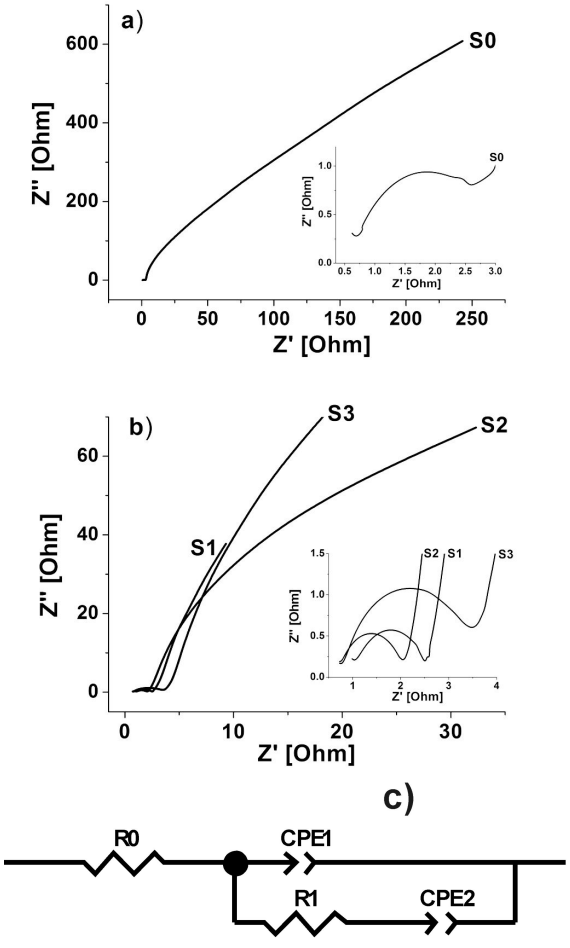

Fig. 8. Nyquist plots of S0 (a) and S1, S2 S3 electrodes (b) (inset: enlarged high-frequency region); an equivalent circuit used for fitting of all electrodes (c)

The electrode based on S1 sample has the lowest proton diffusion resistance in comparison with the other electrodes. The equivalent circuit of the Ni(OH)$_2$-based electrode consists of R_0 (corresponding to the electrolyte and additional contact resistance), R_1 (charge transfer resistance), CPE_1 (capacitance of double electric layer) and CPE_2 (Warburg impedance). These parameters were calculated using experimental Nyquist diagrams with ZView2 software and presented in Table 1.

Table 1. Equivalent scheme parameters for α-Ni(OH)$_2$ and α-Ni(OH)$_2$/C composites electrode

Material	R_0 [Ω]	R_1 [Ω]	CPE_1-T, F	CPE_1-P, F	CPE_2-T [Ω·s$^{-1/2}$]	CPE_2-P
S0	0.51	3.5	0.0057	0.9	0.011	0.63
S1	0.93	1.5	0.0033	0.88	0.325	0.62
S2	0.65	1.7	0.0019	0.89	0.169	0.55
S3	0.71	3.1	0.0033	0.89	0.174	0.75

According to the analysis of EIS data, S1 composite material has the lowest charge transfer resistance and the highest Warburg coefficient. The insertion of carbon into the nickel hydroxide microparticles increased both the electrical conductivity and electrochemical performance of the Ni(OH)$_2$/C composite materials.

4. Conclusions

Simple and effective hydrothermal synthesis of α-Ni(OH)$_2$ and α-Ni(OH)$_2$/carbon composite materials is proposed. It is found that α-Ni(OH)$_2$ particles grow mostly in [0 0 1] crystallographic direction. The formation of conductive carbon cover on Ni(OH)$_2$ particle surfaces of α-Ni(OH)$_2$/C samples is observed. Carbon nanoparticles presence stabilizes α-Ni(OH)$_2$ phase in the alkaline medium that allows one to use Ni(OH)$_2$/carbon composite material as an effective electrode for hybrid supercapacitors with specific capacitance up to 310 F/g. It is found that laser treatment is more acceptable for α-Ni(OH)$_2$/C composite material compared to the ultrasonic one.

References

[1] HEMIY O.M., YABLON L.S., BUDZULYAK I.M., BUDZULYAK S.I., MORUSHKO O.V., KACHMAR A.I., *J. Nano-Electron. Phys.,* 8 (2016), 04074.

[2] ZHONG J.H., WANG A.L., LI G.R., WANG J.-W., OU Y.-N., TONG Y.-X., *J. Mater. Chem.,* 22 (2012), 5656.

[3] PARK J.H., KIM S.W., PARK O.O., KO J.M., *Appl. Phys.,* 82 (2006), 593.

[4] SHYYKO L.O., KOTSYUBYNSKY V.O., BUDZULYAK I.M., SAGAN P., *Nanoscale Res. Lett.,* 11 (2016), 243.

[5] MCEWEN R.S., *J. Phys. Chem.,* 75 (1971), 1782.

[6] BUDZULYAK I.M., IVANICHOK N.YA., RACHIY B.I., VASHCHYNSKY V.M., LISOVSKIY R.P., *Phys. Chem. Solid State,* 16 (2015), 341.

[7] DUAN G.T., CAI W.P., LUO Y.Y., SUN F.Q., *Adv. Funct. Mater.,* 17 (2007), 644.

[8] LUO Y.Y., LI G.H., DUAN G.T., ZHANG L.D., *Nanotechnology,* 17 (2006), 4278.

[9] YANG R., GAO J.L., *Colloid Interface Sci.,* 297 (2006), 134.

[10] LIU L.J., GUAN J.G., SHI W.D., SUN Z., ZHAO J., *J. Phys. Chem.,* 114 (2010), 13565.

[11] DEABATE S., HENN F., DEVAUTOUR S., GIUNTINI J.C., *J. Electrochem. Soc.,* 150 (2003), 23.

[12] RATNER M. A., JOHANSSON P., SHRIVER D. F., *Mater. Res. Soc. Bull.,* 25(3) (2000), 31.

[13] DEABATE S., HENN F., DEVAUTOUR S., GIUNTIN J.C., *J. Electrochem. Soc.,* 150(6), (2003), J23.

[14] DYRE J. C., *J. Appl. Phys.,* 64(5) (1988), 2456.

[15] SHYYKO L., KOTSYUBYNSKY V., BUDZULYAK I., RACHIY B., *Energetika,* 61 (3 – 4) (2015), 36.

[16] LEBOVKA M., GONCHARUK A., BOYKO YU., LISETSKII L., PUCHKOVSKAYA G., *Nanosystems, Nanomaterials, Nanotechnologies,* 7 (2009), 701.

[17] ORESHKIN P.T., *Physics of semiconductors and dielectrics,* Moscow, 1977.

[18] VOLKOV A.A., GORSHUNOV B.P., KOZLOV G.V., *Proc. IOFAN,* 25 (1990), 112.

[19] SHORNIKOVA O.N., MAKSIMOVA N.V., AVDEEV V.V., *A manual for students in the specialty "Composite nanomaterials",* Moscow, 2010.

[20] BODE H., DEHMELT K., WITTE J., *Electrochim. Acta,* 11 (1966), 1079.

[21] MURALIDHARAN V.S., JAYALAKSHMI N., MAGESWARI P., *Bull. Electrochem.,* 7 (1991), 355.

[22] KIANI M.A., MOUSAVI M.F., GHASEMI S., *J. Power Sources,* 195(17) (2010), 5794.

[23] WANG X.Y., YAN J., YUAN H.T., ZHANG Y.-S., SONG D.-Y., *Int. J. Hydrogen Energy,* 24 (1991), 973.

Received 2017-11-22
Accepted 2018-04-23